nature chemical biology

ARTICLES
https://doi.org/10.1038/s41589-020-0641-7

A general strategy to red-shift green fluorescent protein-based biosensors

Shen Zhang and Hui-wang Ai ✉

Compared with green fluorescent protein-based biosensors, red fluorescent protein (RFP)-based biosensors are inherently advantageous because of reduced phototoxicity, decreased autofluorescence and enhanced tissue penetration. However, existing RFP-based biosensors often suffer from small dynamic ranges, mislocalization and undesired photoconversion. In addition, the choice of available RFP-based biosensors is limited, and development of each biosensor requires substantial effort. Herein, we describe a general and convenient method, which introduces a genetically encoded noncanonical amino acid, 3-aminotyrosine, to the chromophores of green fluorescent protein-like proteins and biosensors for spontaneous and efficient green-to-red conversion. We demonstrated that this method could be used to quickly expand the repertoire of RFP-based biosensors. With little optimization, the 3-aminotyrosine-modified biosensors preserved the molecular brightness, dynamic range and responsiveness of their green fluorescent predecessors. We further applied spectrally resolved biosensors for multiplexed imaging of metabolic dynamics in pancreatic β-cells.

Fluorescent protein (FP)-based biosensors are indispensable research tools[1,2]. Despite RFP-based biosensors increasingly being reported, the emission of most existing FP-based biosensors still falls in the green or yellow spectral region[2], where their spectral overlap hinders and sometimes precludes multiplexing. Moreover, because of their use of longer-wavelength excitation light, RFP-based biosensors are expected to reduce phototoxicity and autofluorescence and increase photon penetration and imaging depth. However, RFP-based biosensors are repeatedly outperformed by their green fluorescent counterparts in real applications, due to the remaining shortcomings of existing RFP-based biosensors, such as small dynamic ranges, mislocalization and undesired photoconversion[2]. In this context, there is a pressing need to expand RFP-based biosensors not only for a broader range of analytical targets but also for improved properties.

Although several green-to-red, photoconvertible FPs have been reported and widely used[1], there has been limited success in directly converting a typical green FP (GFP) to an RFP. In one study, mutagenesis of GFP resulted in an 'R10-3' mutant containing a mixture of green and red fluorescent chromophores[3]. A few other studies reported green-to-red photoconversion under anaerobic conditions[4,5], under extensive ultraviolet or blue irradiation with high GFP expression levels[6,7] or in the presence of electron receptors[8,9]. Nevertheless, these approaches usually led to only partial photoconversion. Research has also been done to modify the photophysical properties of FPs with noncanonical amino acids (ncAAs). In one example, by using auxotrophic *Escherichia coli* host strains, a tryptophan analog was incorporated into cyan FP to derive a 'gold' FP, GdFP, with excitation and emission maxima at 466 and 574 nm, respectively[10]. In several other examples, by expressing orthogonal transfer RNAs and aminoacyl-tRNA synthetases (aaRSs) in live cells[11], ncAAs were site-specifically introduced into GFP in response to a nonsense amber codon, resulting in GFP mutants with shifted excitation and emission[12,13], altered pH responses[14,15], photoactivation or photoswitching properties[16–18], or new capabilities to sense various analytes[19–23]. Despite this progress, there is no reliable evidence that any of the aforementioned methods can be generalized for green-to-red conversion of diverse GFP-like proteins and their derived biosensors.

In the process of modifying GFP with 3-aminotyrosine (aY; Fig. 1a) for the development of new biosensors, we serendipitously discovered that aY, when introduced into the chromophores of GFP-like proteins and biosensors via genetic code expansion[11], could spontaneously and efficiently red-shift their fluorescence. Here, we demonstrate that this method can be generalized to red-shift various FP variants and biosensors. In addition to molecular brightness, the dynamic range and responsiveness of the converted biosensors were largely retained. By using spectrally resolved biosensors resulting from this study, we further monitored metabolic dynamics in pancreatic β-cells in response to high glucose.

Results

Genetic encoding of aY in *E. coli* and mammalian cells. A previous study reported a *Methanococcus jannaschii* tyrosyl-tRNA synthetase (*Mj*TyrRS) mutant for the genetic encoding of aY in *E. coli*[24], so we first tested this *Mj*TyrRS mutant but unfortunately observed a high cross-reactivity with tyrosine. Next, we examined another *Mj*TyrRS mutant, which was initially engineered for the genetic encoding of 3-iodotyrosine (ref. [25]). We chose this mutant as our starting point for further engineering, since aY is structurally close to 3-iodotyrosine and this particular *Mj*TyrRS mutant was shown not to esterify tyrosine[25]. We computationally docked aY into the active site of this enzyme and introduced in silico randomization by following our previous procedure[26]. We identified a promising *Mj*TyrRS mutant (designated *Mj*aYRS) with serine at residue 70, which mutation may promote hydrogen bonding with the side-chain amino group of aY (Supplementary Fig. 1a). Next, we expressed a superfolder GFP (sfGFP)[27] mutant with an amber codon introduced to its residue 66 in the presence of *Mj*aYRS and the corresponding amber suppression tRNA. We observed strong fluorescence and obtained the full-length protein in good yield (~6.7 mg per liter of culture) when aY was supplemented (Supplementary Fig. 1b–d).

Center for Membrane and Cell Physiology, Department of Molecular Physiology and Biological Physics, Department of Chemistry, and the UVA Cancer Center, University of Virginia, Charlottesville, VA, USA. ✉e-mail: huiwang.ai@virginia.edu

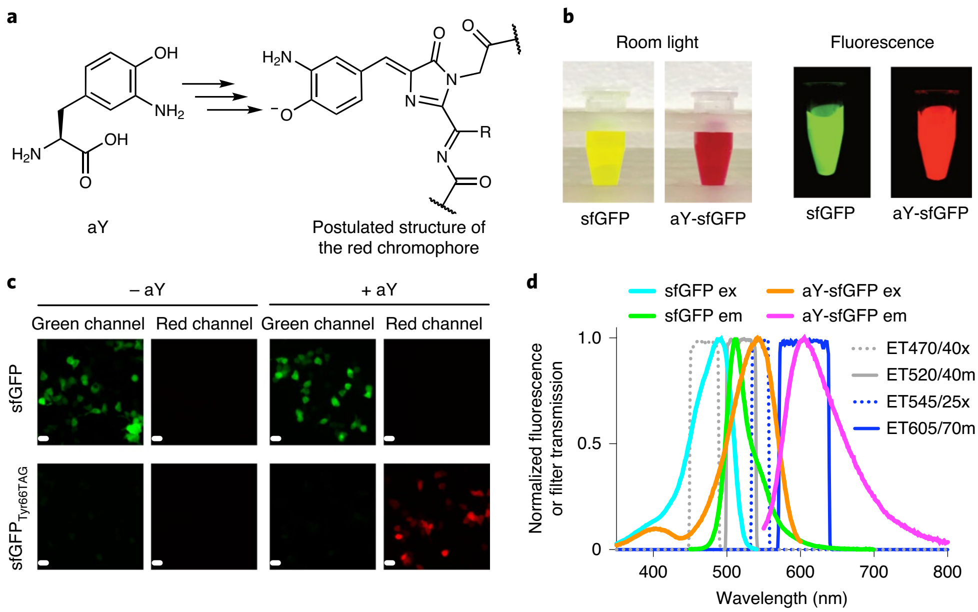

Fig. 1 | Green-to-red conversion of sfGFP by aY. a, Chemical structure of aY and the postulated structure of the chromophores in the aY-converted red FPs. **b**, Imaging of sfGFP and aY-sfGFP proteins prepared from *E. coli*. **c**, Microscopic imaging of HEK 293T cells cotransfected with pMAH-*Ec*aYRS and pcDNA3-sfGFP or pcDNA3-sfGFP(Tyr66TAG) in the presence or absence of aY, showing red fluorescence of aY-sfGFP in mammalian cells. Images were identically treated, except that 100-ms and 300-ms exposures were used to acquire images in the top and bottom rows, respectively. Scale bar, 20 µm. **d**, Fluorescence excitation and emission spectra of sfGFP (cyan and green) and aY-sfGFP (orange and magenta), suggesting that sfGFP and aY-sfGFP can be sequentially imaged with little crosstalk using appropriate filters. Transmission spectra for excitation and emission filters designated with Chroma Technology part numbers are also plotted (gray and blue). Experiments in panels **b**–**d** were repeated three times with similar results using independent biological samples. em, emission; ex, excitation; ET470/40x, ET520/40m, ET545/25x, and ET605/70m are Chroma Technology part numbers for individual filters..

In the absence of aY, little protein was obtained (Supplementary Fig. 1c), suggesting that *Mj*aYRS has satisfactory specificity. In addition, we characterized the protein prepared in the presence of aY with electrospray ionization mass spectrometry (ESI-MS) and confirmed the incorporation of aY to sfGFP (Supplementary Fig. 1e). We did not observe a peak corresponding to sfGFP with tyrosine at residue 66, further confirming the specificity of *Mj*aYRS.

To enable the genetic encoding of aY in mammalian cells, we took *E. coli* tyrosyl-tRNA synthetase (*Ec*TyrRS) as our starting template (Supplementary Fig. 2a). We first introduced a D265R mutation to increase anticodon recognition by the aaRS[28], and further inserted a tyrosine editing domain into *Ec*TyrRS to reduce its reactivity with tyrosine[29]. We next created 30 *Ec*TyrRS variants by mutating residues 37 and 195 within the amino acid substrate-binding pocket. We identified an aaRS variant (also known as *Ec*aYRS) with Y37L and Q195S mutations (Supplementary Fig. 2b) by screening the *Ec*TyrRS mutants for amber suppression of an enhanced GFP (EGFP) gene containing a TAG codon at residue 39. In the presence of aY, *Ec*aYRS and the corresponding tRNA, full-length EGFP was generated in human embryonic kidney (HEK) 293T cells, as confirmed by both fluorescence microscopy and ESI-MS (Supplementary Fig. 2c–e). Although we observed weak fluorescence from the cells cultured in the absence of aY (Supplementary Fig. 2b,c), the ESI-MS analysis of the protein prepared in the presence of aY did not show any peak corresponding to EGFP with tyrosine at residue 39 (Supplementary Fig. 2d), suggesting that *Ec*TyrRS has adequate specificity and aY can outcompete tyrosine for *Ec*TyrRS-catalyzed tRNA aminoacylation.

aY-induced red-shift of FPs and FP-based biosensors. The color of aY-sfGFP (sfGFP[27] with aY introduced to its chromophore-forming residue 66) from *E. coli* was surprisingly red under either room light or green excitation, and it had nearly no residual green fluorescence (Fig. 1b). To test whether this phenomenon is species-specific, we expressed aY-sfGFP in HEK 293T cells and also observed spontaneous, red fluorescence (Fig. 1c). The excitation and emission maxima of aY-sfGFP were red-shifted from those of sfGFP by 56 and 95 nm, respectively, suggesting that it may be possible to pair aY-sfGFP with GFPs or GFP-based biosensors for sequential, dual-color imaging using common fluorescence microscope setups (Fig. 1d).

The chromophore of GFP is spontaneously formed through cyclization, dehydration and oxidation of an internal tripeptide motif, while the chromophores of common RFPs differ from GFP in terms of additional, self-catalyzed oxidation which expands chromophore conjugation via a hydrolyzable *N*-acylimine substitution[30]. Because aY is sensitive to oxidation, we hypothesize that aY-sfGFP spontaneously forms an RFP-like chromophore through additional oxidation (Fig. 1a and Supplementary Fig. 3a). Although the detailed mechanism remains to be explored, the formation of a hydrolyzable chromophore is supported by backbone cleavage of aY-sfGFP under denaturing conditions (Supplementary Fig. 3b). Furthermore, the absorbance of aY-sfGFP decreases at ~540 nm with concurrent increase at ~390 nm as pH drops from neutral to acidic (Supplementary Fig. 3c), suggesting the existence of an anionic chromophore in aY-sfGFP at neutral conditions.

Next, we introduced aY to the chromophores of several FPs containing tyrosine-derived chromophores, including teal fluorescent mTFP1 (ref. [31]), yellow fluorescent Citrine[32], a circularly permuted sfGFP (cpsGFP)[33] and a circularly permuted yellow FP (cpYFP)[23]. Red-shifted excitation and emission were observed for all of them (Extended Data Fig. 1 and Table 1), indicating that the aY-induced green-to-red conversion is neither protein-specific nor topology-specific.

We further determined the molecular brightness of these proteins. Although the quantum yields of the aY-modified proteins

Table 1 | Photophysical properties of the selected FPs

	Chromophore-forming residues	Normal proteins				Proteins with aY-derived chromophores				Brightness ratios[e]
		λ_{ex}[a] (nm)	λ_{em}[b] (nm)	ε (mM^{-1} cm^{-1})[c]	φ[d]	λ_{ex}[a] (nm)	λ_{em}[b] (nm)	ε (mM^{-1} cm^{-1})[c]	φ[d]	
sfGFP	TYG	485	510	85.6	0.70	541	605	125.1	0.43	89.8%
cpsGFP[f]	TYG	488	510	73.1	0.66	527	615	88.5	0.40	73.4%
mTFP1	AYG	462	492	65.6	0.81	514	581	85.5	0.50	80.5%
cpYFP[g]	GYG	503	515	76.3	0.58	569	609	82.6	0.38	70.9%
Citrine	GYG	516	529	75.3	0.75	565	624	95.0	0.45	75.7%

[a]Wavelength of the excitation peak. [b]Wavelength of the emission peak. [c]Extinction coefficient. [d]Quantum yield. [e]Molecular brightness (defined as $\varepsilon \times \varphi$) of an aY-modified protein presented as the percentage of the molecular brightness of the corresponding normal protein. [f]Circularly permuted sfGFP variant previously used to derive the hydrogen sulfide sensor, hsGFP[33]. [g]Circularly permuted EYFP variant previously used to derive the hydrogen sulfide sensor, cpGFP-pAzF[23].

Table 2 | Photophysical properties of the tested genetically encoded biosensors and their aY-modified variants

Biosensor	Analytical target	λ_{ex}[a] (nm)	λ_{em}[b] (nm)	Dynamic Range[c] (%)	ε[d] (mM^{-1} cm^{-1})		φ[e]	
					−	+	−	+
G-GECO1 (ref. [34])	Ca^{2+}	497	512	1,983	4.7	68.1	0.26	0.38
aY-G-GECO1	Ca^{2+}	528	594	1,566	7.7	79.9	0.14	0.22
ZnGreen1 (ref. [35])	Zn^{2+}	474	500	2,531	24.8	1.3	0.48	0.35
aY-ZnGreen1	Zn^{2+}	520	585	915	34.7	4.8	0.28	0.20
iGluSnFR[36]	glutamate	488	510	257	9.6	32.6	0.58	0.60
aY-iGluSnFR	glutamate	528	600	270	12.2	42.7	0.46	0.49
iGABASnFR[37]	GABA	502	513	143	ND[f]	ND[f]	ND[f]	ND[f]
aY-GABASnFR	GABA	541	602	92	ND[f]	ND[f]	ND[f]	ND[f]
dLight1.2 (ref. [38])	dopamine	496	513	194	ND[f]	ND[f]	ND[f]	ND[f]
aY-dLight1.2	dopamine	545	603	117	ND[f]	ND[f]	ND[f]	ND[f]
SoNar[39]	NAD^+/NADH	497	512	257 [2,532][g]	7.6	23.0	0.44	0.51
aY-SoNar	NAD^+/NADH	544	604	426 [2,656][g]	6.5	28.6	0.29	0.35
iNap1 (ref. [40])	NADPH	497	513	82 [273][g]	22.6	13.1	0.50	0.43
aY-iNap1	NADPH	545	604	614 [11,735][g]	27.6	4.4	0.41	0.36
PercevalHR[41]	ATP	498	513	155 [364][g]	14.6	35.6	0.28	0.28
aY-PercevalHR	ATP	545	604	117 [650][g]	18.4	40.5	0.21	0.21
iATPSnFR1.1 (ref. [42])	ATP	493	513	106	22.6	43.9	0.36	0.37
aY-iATPSnFR1.1	ATP	541	608	75	29.1	50.9	0.28	0.28

[a]Wavelength of the excitation peak near 490 and 540 nm for green and aY-modified, red fluorescent biosensors, respectively. [b]Wavelength of the emission peak. [c]Unless otherwise specified, dynamic range is defined as the intensiometric change ($\Delta F/F_{min}$) around emission peaks in the presence of 480- and 540-nm excitation for green and aY-modified, red fluorescent biosensors, respectively. [d]Extinction coefficient in the presence (+) or absence (−) of the corresponding analyte. For SoNar and aY-SoNar, presented are values with NAD^+ (+) or NADH (−). [e]Quantum yield. [f]Not determined. [g]In square brackets are dynamic ranges of the sensors operated in the excitation-ratiometric mode; defined as R_{max}/R_{min}, the maximal intensity ratio over the minimal intensity ratio at two excitation peak wavelengths.

were reduced by ~40%, their extinction coefficients were increased by 8–46%, resulting in overall molecular brightness ranging from 70% to 90% of their parental proteins with tyrosine-derived chromophores (Table 1). This phenomenon is striking because no individual optimization was performed with these aY-modified proteins.

After confirming that aY can red-shift various tyrosine-derived chromophores, we used aY to modify a number of biosensors based on circularly permuted green, teal or yellow FPs, including G-GECO1 (a Ca^{2+} sensor)[34], ZnGreen1 (a Zn^{2+} sensor)[35], iGluSnFR (a glutamate sensor)[36], iGABASnFR (a GABA (γ-aminobutyric acid) sensor)[37], dLight1.2 (a dopamine sensor)[38], SoNar (an NAD^+/NADH sensor)[39], iNAP1 (an NADPH sensor)[40], PercevalHR (an ATP sensor)[41] and iATPSnFR1.1 (another ATP sensor)[42]. We observed red-shifted fluorescence for all tested biosensors (Table 2). Without individual optimization, the aY-modified biosensors again inherited most of the molecular brightness from their green fluorescent predecessors (Table 2). Moreover, the converted biosensors largely preserved the dynamic range and responsiveness, as shown in our validation experiments with purified proteins, cultured mammalian cell lines and/or primary neurons (Extended Data Figs. 2–9 and Supplementary Videos 1 and 2). In particular, we used the green fluorescent G-GECO1 sensor and aY-iGluSnFR for dual-color imaging of Ca^{2+} and glutamate in mouse neurons during membrane depolarization and confirmed the spectral orthogonality of the two biosensors (Extended Data Fig. 4 and Supplementary Video 2). Some biosensors, such as SoNar, iNap1 and PercevalHR, are known for robust, excitation-ratiometric responses[39–41]. Not surprisingly, their aY-modified biosensors were also excitation-ratiometric (Extended Data Figs. 7–9). The dynamic range of these biosensors,

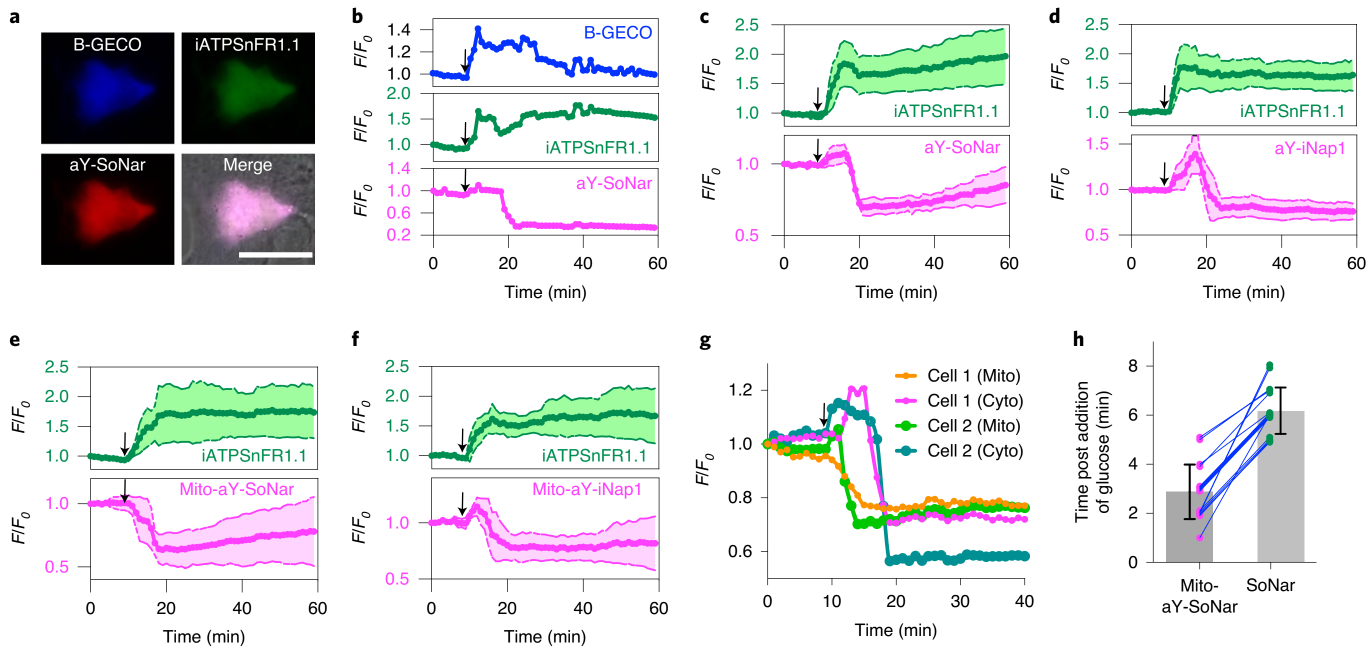

Fig. 2 | Fluorescence imaging of glucose-induced metabolic dynamics in pancreatic MIN6 β-cells. a, Representative tri-color images of MIN6 coexpressing B-GECO, iATPSnFR1.1 and aY-SoNar. $n=3$ repeats. Scale bar, 20 µm. Similar results were gained with three independent repeats. **b**, Representative traces (F/F_0) for B-GECO, iATPSnFR1.1 and aY-SoNar. Similar results were gained with three independent repeats. **c**, Quantitative traces (F/F_0) for coexpressed iATPSnFR1.1 and aY-SoNar ($n=8$ cells examined over three independent experiments). **d**, Quantitative traces (F/F_0) for coexpressed iATPSnFR1.1 and aY-iNap1 ($n=7$ cells examined over three independent experiments). **e**, Quantitative traces (F/F_0) for coexpressed iATPSnFR1.1 and mitochondrial aY-SoNar ($n=8$ cells examined over three independent experiments). **f**, Quantitative traces (F/F_0) for coexpressed iATPSnFR1.1 and mitochondrial aY-iNap1 ($n=12$ cells examined over three independent experiments). **g**, Representative traces (F/F_0) for two cells coexpressing cytosolic SoNar and mitochondrial aY-SoNar. Similar results were obtained with five independent repeats. **h**, Comparison of response time (corresponding to the middle point of the fluorescence decrease phase) in individual MIN6 cells after glucose addition ($n=17$ cells examined over five independent experiments; Mito-aY-SoNar: 2.88 ± 1.11 min; SoNar: 6.18 ± 0.95 min; Wilcoxon matched-pairs signed rank test, $P=0.00015$). The time points for addition of 20 mM D-glucose are shown as arrows in panels **b**–**g**. Data are presented as mean and s.d. of indicated replicates. F/F_0, fluorescence intensity at a given time over the intensity at the start of the experiment.

by analyzing either intensiometric changes ($\Delta F/F_{min}$, the amplitude of the fluorescence change over the minimal fluorescence intensity) around their emission peaks in the presence of 540 nm excitation or ratiometric changes concerning the two excitation peaks, was comparable to or even better than that of the wild-type sensors harboring tyrosine-derived chromophores (Table 2).

Imaging of metabolic dynamics in pancreatic β-cells. To further demonstrate the use of aY-modified biosensors for multiplexed imaging, we monitored glucose-induced metabolic dynamics in mouse MIN6 β-cells. Pancreatic β-cells are responsible for glucose sensing and secretion of insulin, a key hormone regulating sugar metabolism. Upon entering β-cells, glucose breaks down to generate an array of metabolic signals that regulate insulin synthesis and secretion (Supplementary Fig. 4). Although previous studies have demonstrated important roles of NADH, NADPH, ATP and Ca^{2+} in glucose sensing in β-cells, the spatiotemporal dynamics of these signals has not been fully understood[43]. We first coexpressed B-GECO (a blue fluorescent Ca^{2+} biosensor)[34], iATPSnFR1.1 (a green fluorescent ATP biosensor)[42] and aY-SoNar (a red fluorescent NAD^+/NADH biosensor) in MIN6 cells (Fig. 2a). To simplify the multicolor time-lapse imaging process and reduce the overall light exposure to avoid photobleaching and phototoxicity, we focused on only the intensiometric changes of the biosensors. In response to high glucose (20 mM), we observed an immediate rise of B-GECO or iATPSnFR1.1 fluorescence, reflecting an acute increase of intracellular Ca^{2+} and ATP (Fig. 2b). The fluorescence of B-GECO or iATPSnFR1.1 was sustained at high levels with some expected oscillations for an extended period. Surprisingly, the fluorescence of aY-SoNar displayed a small, immediate increase followed by a drop, suggesting an initial small increase and then a decrease of cellular NAD^+/NADH. Despite the heterogeneity of individual MIN6 cells, this trend for aY-SoNar was well-reproduced when we examined more cells. (Fig. 2c). Similarly, we observed a phenomenal rise followed by a reduction of the fluorescence of aY-iNap1 (a red fluorescent NADPH biosensor) post glucose stimulation (Fig. 2d). Since the concentration of NADPH is inversely correlated with the fluorescence of aY-iNap1 (Extended Data Fig. 7), we interpret that high glucose transiently decreased NADPH and then maintained high NADPH levels in MIN6 cells.

Because NAD^+/NADH and NADPH are compartmentalized and mitochondria play a central role in metabolism, we next fused aY-SoNar or aY-iNap1 to a mitochondrial localization sequence for expression in the mitochondria of MIN6 cells. In response to high glucose, mitochondrial NAD^+/NADH displayed an immediate decrease, whereas mitochondrial NADPH still decreased transiently before the rise (Fig. 2e,f). We further coexpressed SoNar and mitochondrial aY-SoNar to follow compartmentalized changes in the same MIN6 cells (Fig. 2g, Extended Data Fig. 10 and Supplementary Video 3). Upon glucose stimulation, there were obvious and consistent delays in cytosolic NAD^+/NADH decrease compared with mitochondrial NAD^+/NADH, and the average delay time was determined to be 3.3 min by analyzing 17 individual cells (Fig. 2g,h). To exclude the possibility that the observed time differences may be caused by different response kinetics, we monitored the fluorescence of SoNar, iNap1, iATPSnFR1.1 and their aY-modified variants upon sequential injections of the corresponding analytes and analyte-depleting enzymatic mixtures (Supplementary Fig. 5). The sensor responses, which were certainly convoluted by the speed of reagent dispensing and mixing, occurred and completed within a few seconds and were much faster than the time differences discussed above regarding our β-cell imaging experiments (Fig. 2c,d,f–h).

Discussion

In this study, we engineered two aaRSs to genetically encode aY in *E. coli* and mammalian cells. Both *Mj*aYRS and *Ec*TyrRS showed adequate specificity for site-specific incorporation of aY into proteins. We further developed a general method based on the introduction of aY to the chromophores of GFP-like proteins and biosensors for spontaneous and efficient green-to-red conversion. Our approach does not require photoconversion or other special experimental conditions and is compatible with a variety of FPs and FP-based biosensors in *E. coli*, mammalian cell lines and primary cells. Therefore, this method can be used to quickly expand RFP-based biosensors. Although ncAAs have been explored previously for spectral shifting of FPs, aY is unique in that it causes drastic red-shifting and, with little optimization, the molecular brightness of the resultant FPs and biosensors was largely retained. Moreover, the aY-modified biosensors mostly preserved the dynamic range and responsiveness of their green fluorescent predecessors.

Despite its promise, this technology has a few limitations. First, amber codon suppression is used here to achieve genetic code expansion; although this process is often tolerated by live organisms[11], we expect potential side effects such as hijacking of amber codons in host genomes. In addition, the suppression of the amber codon introduced into the genes of the FPs or biosensors is incomplete due to the competition between amber suppression and release-factor-induced translation termination, and thus, we must use longer exposure times to image aY-modified FPs and biosensors, or increase the amount of the plasmids for the expression of aY-modified proteins to gain similar protein expression levels in cells. Furthermore, the amino acid aY has to be exogenously provided into cell culture media, so there may be challenges to using aY-modified biosensors for in vivo imaging. Fortunately, several previous studies have utilized genetic code expansion systems in multi-cellular organisms, such as worms, fruit flies, zebrafish and mice[44–46], and these studies may serve as examples for further adaption of aY-modified biosensors into similar organisms.

We utilized the aY-based strategy to red-shift a panel of biosensors, including those for metal ions, neurotransmitters and cell metabolites. Some biosensors were excitation-ratiometric before the conversion and they remained excitation-ratiometric after the conversion. The aY modification drastically red-shifted the long-wavelength excitation band of these biosensors, but only slightly red-shifted their short-wavelength excitation band. Thus, to operate the converted biosensors in a ratiometric mode, ~420-nm excitation would still be needed. Therefore, although ratiometric imaging is expected to be advantageous in terms of quantitation, in our microscopic imaging experiments we operated the biosensors intensiometrically, with only the long-wavelength excitation, for simplicity and reduced phototoxicity and photobleaching.

We further used these biosensors for multiplexed imaging of metabolic dynamics in pancreatic β-cells. As expected, we observed an increase in cellular ATP and Ca^{2+} in response to high glucose. However, changes in NAD^+/NADH and NADPH levels were more complicated. Normally, a net gain in NADH is expected to occur upstream to the gain in ATP in glucose metabolism (Supplementary Fig. 4)[43]. However, we observed a delay in high-glucose-induced NADH increase, particularly in the cytosol, in relation to ATP increase. This unexpected delay corroborates the notion that glucose-sensing mechanisms in β-cells are not yet fully understood[43,47]. On the basis of our imaging results, we postulate that, in the first few minutes after high-glucose stimulation, there may be transient ATP production from NADH using enzymes such as lactate dehydrogenase, or high glucose and its derivatives may activate metabolic shuttles between the cytosol and mitochondria[43,47]. In addition, glucose-induced NADPH was previously suggested to protect β-cells from oxidative stress[48], but our study uncovered an unexpected, transient phase lasting a few minutes post glucose stimulation, during which NADPH decreases in both cytosol and mitochondria of MIN6 cells. The result suggests that transient oxidation, likely caused by NADPH oxidase or mitochondrial reactive oxygen species[49,50], may be an acute signaling response of β-cells to high glucose. Research is ongoing in our laboratory to further investigate these mechanisms using primary β-cells and islets.

Online content

Any methods, additional references, Nature Research reporting summaries, source data, extended data, supplementary information, acknowledgements, peer review information; details of author contributions and competing interests; and statements of data and code availability are available at https://doi.org/10.1038/s41589-020-0641-7.

Received: 3 February 2020; Accepted: 6 August 2020;
Published online: 14 September 2020

References

1. Rodriguez, E. A. et al. The growing and glowing toolbox of fluorescent and photoactive proteins. *Trends Biochem. Sci.* **42**, 111–129 (2017).
2. Greenwald, E. C., Mehta, S. & Zhang, J. Genetically encoded fluorescent biosensors illuminate the spatiotemporal regulation of signaling networks. *Chem. Rev.* **118**, 11707–11794 (2018).
3. Mishin, A. S. et al. The first mutant of the *Aequorea victoria* green fluorescent protein that forms a red chromophore. *Biochemistry* **47**, 4666–4673 (2008).
4. Sawin, K. E. & Nurse, P. Photoactivation of green fluorescent protein. *Curr. Biol.* **7**, R606–R607 (1997).
5. Elowitz, M. B., Surette, M. G., Wolf, P. E., Stock, J. & Leibler, S. Photoactivation turns green fluorescent protein red. *Curr. Biol.* **7**, 809–812 (1997).
6. Sattarzadeh, A., Saberianfar, R., Zipfel, W. R., Menassa, R. & Hanson, M. R. Green to red photoconversion of GFP for protein tracking in vivo. *Sci. Rep.* **5**, 11771 (2015).
7. Ai, M. et al. Green-to-red photoconversion of GCaMP. *PLoS ONE* **10**, e0138127 (2015).
8. Bogdanov, A. M. et al. Green fluorescent proteins are light-induced electron donors. *Nat. Chem. Biol.* **5**, 459–461 (2009).
9. Saha, R. et al. Light driven ultrafast electron transfer in oxidative redding of green fluorescent proteins. *Sci. Rep.* **3**, 1580 (2013).
10. Bae, J. H. et al. Expansion of the genetic code enables design of a novel 'gold' class of green fluorescent proteins. *J. Mol. Biol.* **328**, 1071–1081 (2003).
11. Liu, C. C. & Schultz, P. G. Adding new chemistries to the genetic code. *Annu. Rev. Biochem.* **79**, 413–444 (2010).
12. Wang, L., Xie, J., Deniz, A. A. & Schultz, P. G. Unnatural amino acid mutagenesis of green fluorescent protein. *J. Org. Chem.* **68**, 174–176 (2003).
13. Wang, L. et al. Significant expansion and red-shifting of fluorescent protein chromophore determined through computational design and genetic code expansion. *Biophys. Rep.* **4**, 273–285 (2018).
14. Villa, J. K. et al. Fluorescence modulation of green fluorescent protein using fluorinated unnatural amino acids. *Molecules* **22**, 1194 (2017).
15. Fu, C. et al. Genetically encoding quinoline reverses chromophore charge and enables fluorescent protein brightening in acidic vesicles. *J. Am. Chem. Soc.* **140**, 11058–11066 (2018).
16. Groff, D., Wang, F., Jockusch, S., Turro, N. J. & Schultz, P. G. A new strategy to photoactivate green fluorescent protein. *Angew. Chem. Int. Ed. Engl.* **49**, 7677–7679 (2010).
17. Reddington, S. C. et al. Different photochemical events of a genetically encoded phenyl azide define and modulate GFP fluorescence. *Angew. Chem. Int. Ed. Engl.* **52**, 5974–5977 (2013).
18. Reddington, S. C. et al. Directed evolution of GFP with non-natural amino acids identifies residues for augmenting and photoswitching fluorescence. *Chem. Sci.* **6**, 1159–1166 (2015).

19. Wang, F., Niu, W., Guo, J. & Schultz, P. G. Unnatural amino acid mutagenesis of fluorescent proteins. *Angew. Chem. Int. Ed. Engl.* **51**, 10132–10135 (2012).
20. Liu, X. et al. Significant expansion of the fluorescent protein chromophore through the genetic incorporation of a metal-chelating unnatural amino acid. *Angew. Chem. Int. Ed. Engl.* **52**, 4805–4809 (2013).
21. Ayyadurai, N. et al. Development of a selective, sensitive, and reversible biosensor by the genetic incorporation of a metal-binding site into green fluorescent protein. *Angew. Chem. Int. Ed. Engl.* **50**, 6534–6537 (2011).
22. Chen, Z. J., Ren, W., Wright, Q. E. & Ai, H. W. Genetically encoded fluorescent probe for the selective detection of peroxynitrite. *J. Am. Chem. Soc.* **135**, 14940–14943 (2013).
23. Chen, S., Chen, Z. J., Ren, W. & Ai, H. W. Reaction-based genetically encoded fluorescent hydrogen sulfide sensors. *J. Am. Chem. Soc.* **134**, 9589–9592 (2012).
24. Seyedsayamdost, M. R., Xie, J., Chan, C. T., Schultz, P. G. & Stubbe, J. Site-specific insertion of 3-aminotyrosine into subunit α2 of *E. coli* ribonucleotide reductase: direct evidence for involvement of Y_{730} and Y_{731} in radical propagation. *J. Am. Chem. Soc.* **129**, 15060–15071 (2007).
25. Sakamoto, K. et al. Genetic encoding of 3-iodo-L-tyrosine in *Escherichia coli* for single-wavelength anomalous dispersion phasing in protein crystallography. *Structure* **17**, 335–344 (2009).
26. Ren, W., Truong, T. M. & Ai, H. W. Study of the binding energies between unnatural amino acids and engineered orthogonal tyrosyl-tRNA synthetases. *Sci. Rep.* **5**, 12632 (2015).
27. Pedelacq, J. D., Cabantous, S., Tran, T., Terwilliger, T. C. & Waldo, G. S. Engineering and characterization of a superfolder green fluorescent protein. *Nat. Biotechnol.* **24**, 79–88 (2006).
28. Takimoto, J. K., Adams, K. L., Xiang, Z. & Wang, L. Improving orthogonal tRNA-synthetase recognition for efficient unnatural amino acid incorporation and application in mammalian cells. *Mol. BioSyst.* **5**, 931–934 (2009).
29. Oki, K., Sakamoto, K., Kobayashi, T., Sasaki, H. M. & Yokoyama, S. Transplantation of a tyrosine editing domain into a tyrosyl-tRNA synthetase variant enhances its specificity for a tyrosine analog. *Proc. Natl Acad. Sci. USA* **105**, 13298–13303 (2008).
30. Gross, L. A., Baird, G. S., Hoffman, R. C., Baldridge, K. K. & Tsien, R. Y. The structure of the chromophore within DsRed, a red fluorescent protein from coral. *Proc. Natl Acad. Sci. USA* **97**, 11990–11995 (2000).
31. Ai, H. W., Henderson, J. N., Remington, S. J. & Campbell, R. E. Directed evolution of a monomeric, bright and photostable version of *Clavularia* cyan fluorescent protein: structural characterization and applications in fluorescence imaging. *Biochem. J.* **400**, 531–540 (2006).
32. Griesbeck, O., Baird, G. S., Campbell, R. E., Zacharias, D. A. & Tsien, R. Y. Reducing the environmental sensitivity of yellow fluorescent protein. Mechanism and applications. *J. Biol. Chem.* **276**, 29188–29194 (2001).
33. Chen, Z. J. & Ai, H. W. A highly responsive and selective fluorescent probe for imaging physiological hydrogen sulfide. *Biochemistry* **53**, 5966–5974 (2014).
34. Zhao, Y. et al. An expanded palette of genetically encoded Ca^{2+} indicators. *Science* **333**, 1888–1891 (2011).
35. Chen, Z. & Ai, H. W. Single fluorescent protein-based indicators for zinc ion (Zn^{2+}). *Anal. Chem.* **88**, 9029–9036 (2016).
36. Marvin, J. S. et al. An optimized fluorescent probe for visualizing glutamate neurotransmission. *Nat. Methods* **10**, 162–170 (2013).
37. Marvin, J. S. et al. A genetically encoded fluorescent sensor for in vivo imaging of GABA. *Nat. Methods* **16**, 763–770 (2019).
38. Patriarchi, T. et al. Ultrafast neuronal imaging of dopamine dynamics with designed genetically encoded sensors. *Science* **360**, eaat4422 (2018).
39. Zhao, Y. et al. SoNar, a highly responsive NAD^+/NADH sensor, allows high-throughput metabolic screening of anti-tumor agents. *Cell Metab.* **21**, 777–789 (2015).
40. Tao, R. et al. Genetically encoded fluorescent sensors reveal dynamic regulation of NADPH metabolism. *Nat. Methods* **14**, 720–728 (2017).
41. Tantama, M., Martinez-Francois, J. R., Mongeon, R. & Yellen, G. Imaging energy status in live cells with a fluorescent biosensor of the intracellular ATP-to-ADP ratio. *Nat. Commun.* **4**, 2550 (2013).
42. Lobas, M. A. et al. A genetically encoded single-wavelength sensor for imaging cytosolic and cell surface ATP. *Nat. Commun.* **10**, 711 (2019).
43. Fridlyand, L. E. & Philipson, L. H. Glucose sensing in the pancreatic beta cell: a computational systems analysis. *Theor. Biol. Med. Model* **7**, 15 (2010).
44. Brown, W., Liu, J. & Deiters, A. Genetic code expansion in animals. *ACS Chem. Biol.* **13**, 2375–2386 (2018).
45. Ernst, R. J. et al. Genetic code expansion in the mouse brain. *Nat. Chem. Biol.* **12**, 776–778 (2016).
46. Wang, L. Engineering the genetic code in cells and animals: biological considerations and impacts. *Acc. Chem. Res.* **50**, 2767–2775 (2017).
47. Korosak, D. & Slak Rupnik, M. Collective sensing of β-cells generates the metabolic code. *Front. Physiol.* **9**, 31 (2018).
48. Gray, J. P., Alavian, K. N., Jonas, E. A. & Heart, E. A. NAD kinase regulates the size of the NADPH pool and insulin secretion in pancreatic β-cells. *Am. J. Physiol. Endocrinol. Metab.* **303**, E191–E199 (2012).
49. Plecitá-Hlavatá, L. et al. Glucose-stimulated insulin secretion fundamentally requires H_2O_2 signaling by NADPH oxidase 4. *Diabetes* **69**, 1341–1354 (2020).
50. Dan Dunn, J., Alvarez, L. A., Zhang, X. & Soldati, T. Reactive oxygen species and mitochondria: a nexus of cellular homeostasis. *Redox Biol.* **6**, 472–485 (2015).

Publisher's note Springer Nature remains neutral with regard to jurisdictional claims in published maps and institutional affiliations.

Methods

Materials, reagents and general methods. Synthetic DNA oligonucleotides were purchased from Eurofins Genomics or Integrated DNA Technologies. The gene fragments for dLight1.2, SoNar and iNap1 were chemically synthesized and purchased from Eurofins Genomics. CMV-B-GECO1 (Addgene plasmid no. 32448) and pTorPE-G-GECO1 (Addgene plasmid no. 32466) were gifts from R. Campbell (University of Alberta). pCMV(MinDis).iGluSnFR (Addgene plasmid no. 41732) and pAAV.hSynap.iGABASnFR (Addgene plasmid no. 112159) were gifts from L. Looger (Janelia). pm-iATPSnFR1.1 (Addgene plasmid no. 102549) was a gift from B. Khakh (University of California, Los Angeles). FUGW-PercevalHR (Addgene plasmid no. 49083) was a gift from G. Yellen (Harvard). Wild-type *Mj*TyrRS and *Ec*TyrRS genes were gifts from P. Schultz (Scripps). ZnGreen1 was previously reported by our laboratory[35]. FastDigest restriction endonucleases and Phusion High-Fidelity DNA Polymerase were purchased from Fisher Scientific. ChoiceTaq DNA polymerase was purchased from Denville Scientific. The aY amino acid (also known as *H*-3-amino-Tyr-OH·2HCl, catalog no. 402789) was purchased from Bachem. 2-Deoxy-D-glucose (also known as 2-DG, catalog no. D0051) and tetramethylazodicarboxamide (also known as diamide, catalog no. A1458) were purchased from TCI America. Dopamine hydrochloride (catalog no. A11136), ionomycin (catalog no. J62448) and NADH (catalog no. J61638) were purchased from Alfa Aesar. *N*,*N*,*N*′,*N*′-tetrakis(2-pyridinylmethyl)-1,2-ethanediamine (also known as TPEN, catalog no. 13340) and β-nicotinamide adenine dinucleotide phosphate reduced tetrasodium salt (also known as NADPH, catalog no. 9000743) were purchased from Cayman Chemical. NAD^+ (catalog no. 481911) was purchased from Sigma-Aldrich. Monosodium L-glutamate (catalog no. GL135) was purchased from Spectrum Chemical. Cell culture media were purchased from Corning. Other chemicals were purchased from Fisher Scientific. DNA sequencing was performed by Eurofins Genomics. Fluorescence images were acquired with a Leica DMi8 inverted microscope equipped with a Leica EL6000 light source and a Photometrics Prime 95B Scientific CMOS camera. Depending on the brightness of individual samples, images were usually acquired with 10–15% of the light source intensity, 100–300-ms exposure and a full-well camera detection mode. A TRITC filter cube with a 545/25-nm-bandpass excitation filter and a 605/70-nm-bandpass emission filter was used to record red fluorescence from aY-modified FPs and biosensors. A fluorescein isothiocyanate (FITC) filter cube with a 470/40-nm-bandpass excitation filter and a 520/40-nm-bandpass emission filter was used to record green fluorescence from corresponding FPs and biosensors. A DAPI filter cube with a 377/50-nm-bandpass excitation filter and a 447/60-nm-bandpass emission filter was used to record blue fluorescence from B-GECO. SDS–PAGE was used to verify the purity of the prepared proteins (Supplementary Fig. 6). Additional unprocessed SDS–PAGE gel scans are presented in Supplementary Fig. 7. Other general information is available from the Nature Research Reporting Summary.

Identification of aaRS for genetic encoding of aY in *E. coli*. Starting with the Protein Data Bank (PDB) entry, 2ZP1, which is an *Mj*TyrRS mutant (*Mj*TyrRS-H70A/D158T/I159S/D286Y) in complex with 3-iodotyrosine (ref. [25]), random mutagenesis at residue 70 was computationally introduced, and the energy score function embedded in Autodock Vina 1.1.2 (ref. [51]) was used to assess the binding free energies of all complexes. By following our previously reported procedure[26], a promising *Mj*TyrRS mutant with H70S, D158T, I159S and D286Y mutations (designated *Mj*aYRS) was identified. These mutations were next experimentally introduced into the wild-type *Mj*TyrRS by using sequential overlap PCR reactions and the resultant gene fragment was ligated into the previously reported pEvol plasmid[52]. Next, pEvol-*Mj*aYRS and pBAD-sfGFP(Tyr66TAG) were used to cotransform bacterial DH10B cells. A colony picked from LB agar plates supplemented with ampicillin ($100\,\mu g\,ml^{-1}$) and chloramphenicol ($50\,\mu g\,ml^{-1}$) was used to inoculate 2 ml of LB medium at 37 °C. The next day, the saturated culture was added to 100 ml of LB medium. When optical density at 600 nm reached 0.6, L-arabinose (0.2%, w/v) and the aY amino acid (2 mM) were added to induce protein expression. After two additional days of shaking incubation at 250 r.p.m. and 30 °C, cells were pelleted and lysed with sonication. A control sample without aY was simultaneously prepared. Fluorescence of cleared cell lysates was analyzed. Strong red fluorescence was observed only for the positive group to which aY was added during protein expression. Ni-NTA agarose beads (Thermo Scientific) were added to remaining lysates and 6xHis-tagged proteins were purified by following the manufacturer's instructions. Proteins eluted from Ni-NTA beads were analyzed with SDS–PAGE and a band matching the size of full-length sfGFP was observed. Moreover, the eluted protein was desalted by precipitation with methanol and chloroform. The protein pellet was dissolved in ddH_2O supplemented with 1% formic acid and injected into a Waters SQD2 electrospray ionization mass spectrometer. The molar mass of the intact protein was determined by deconvolution of ESI peaks in MagTran1.03 (ref. [53]).

Identification of aaRS for genetic encoding of aY in mammalian cells. On the basis of the PDB entry 1WQ3, which is an *Ec*TyrRS mutant in complex with 3-iodotyrosine (ref. [54]), residues 37 and 195 of *Ec*TyrRS were identified for mutagenesis. First, a D265R mutation was introduced to *Ec*TyrRS using overlap PCR because this mutation was reported to increase anticodon recognition by the aaRS[28]. Furthermore, a gene fragment encoding the tyrosine editing domain of phenylalanyl-tRNA synthetase (PheRS)[29] was purchased from Eurofins Genomics and inserted into *Ec*TyrRS via overlap PCRs, resulting in *Ec*TyrRS* for reduced activity toward tyrosine. Using the aforementioned *Ec*TyrRS* as the template, overlap PCRs were used to introduce mutations to residues 37 and 195 (numbered according to the wild-type *Ec*TyrRS) and a total of 30 variants (residue 37: A, S, I, T, L or V; and residue 195: A, N, S, T or C) in the pMAH vector[23,55] were generated. These pMAH plasmids were used to cotransfect HEK 293T cells with pcDNA3-EGFP(Tyr39TAG) (refs. [23,55]). The aY amino acid (2 mM) was supplemented to cell culture media. After 2 d of incubation, cell lysates were prepared and their fluorescence was determined by using a BioTek Synergy Mx plate reader. By comparing the lysate fluorescence of cells cultured in the presence and absence of the aY amino acid, an *Ec*TyrRS* mutant with the highest incorporation specificity and efficiency was identified. This pMAH-aYRS plasmid was again used to cotransfect HEK 293T cells with pcDNA3-EGFP(Tyr39TAG), and the fluorescence difference of HEK 293T in the presence and absence of aY was confirmed with fluorescence microscopy. Furthermore, the full-length EGFP was purified using Ni-NTA agarose beads, desalted and analyzed by ESI-MS as described in the previous paragraph for the sfGFP protein prepared from *E. coli*.

Detection of aY-sfGFP fragmentation using SDS–PAGE. Following a previously reported method[30], purified aY-sfGFP in 1x SDS gel-loading buffer was either unboiled or boiled at 100 °C for 10 min, before being loaded onto a 15% SDS polyacrylamide gel. Similarly treated mCherry and sfGFP were used for comparison. After electrophoresis, the gel was stained with Coomassie blue R-250.

Construction of expression vectors for FPs and biosensors. Briefly, overlap PCRs with mutagenic primers were used to replace the codon of the chromophore tyrosine with the amber codon (TAG). The assembled gene fragments were inserted into either pBAD/Myc-His between Xho I and Hind III restriction sites for *E. coli* expression, or pcDNA3 between Hind III and Xho I restriction sites for mammalian expression. To express the amber variants of iGABASnFR and iGluSnFR on the mammalian cell surface, the gene fragments were inserted to pDisplay between Bgl II and Sal I restriction sites. In addition, two residues of SoNar, iNap1 and PercevalHR corresponding to residues 68 and 69 of wild-type GFP were mutated to V and M, respectively, because these mutations were found to promote the formation of the red chromophore. For comparison purposes, pBAD/Myc-His, pcDNA3 and/or pDisplay plasmids harboring the genes of wild-type FPs and biosensors were created in parallel. To express biosensors such as SoNar in mitochondria, overlap PCRs were used to add an N-terminal mitochondrial localization sequence (MLSLRQSIRFFKPATRTLCSSRYLL) and the resultant gene fragments were inserted into pcDNA3 between Hind III and Xho I.

Spectral characterization of biosensors. Wild-type and aY-modified G-GECO1, ZnGreen1, iGluSnFR, SoNar, iNap1, PercevalHR and iATPSnFR1.1 in pBAD/Myc-His were purified as C-terminal His_6-tagged proteins from *E. coli* DH10B as previously described[22]. Furthermore, the proteins were passed through a HiPrep Sephacryl S-200 HR gel filtration column (GE Healthcare) by using elution buffers (10 mM MOPS, pH 7.2 and 100 mM KCl for G-GECO1 and its aY-modified variant; 150 mM HEPES, pH 7.4, 100 mM NaCl and 0.5 mM TCEP for ZnGreen1 and its aY-modified variant; and 50 mM Tris HCl, pH 7.4 and 100 mM NaCl for other biosensors). The Bradford assay was used to determine protein concentrations. Sensor proteins were further diluted with their corresponding elution buffers to the final concentrations of ~100 nM and then mixed with other desired components for measurement of fluorescence excitation and emission spectra on a monochromator-based BioTek Synergy Mx plate reader. To determine extinction coefficients, absorbance was measured on a BioTek Synergy Mx plate reader and corrected for 1-cm light path, and the values for extinction coefficients were then calculated using Beer's law. To determine quantum yields, fluorescein dissolved in ethanol ($\varphi = 0.79$)[56] or purified mScarlet-I protein ($\varphi = 0.54$)[57] was used as the standard. The full emission spectrum of each protein was measured with 1-nm resolution, and intensity values were then added up, normalized to absorbance at the excitation wavelength and compared with the corresponding references. Spectral characterizations of dLight1.2 and iGABASnFR were directly performed with HEK 293T cells. After transfection and sensor expression, ~1 million cells were dissociated and thoroughly rinsed with Dulbecco's PBS (DPBS). Next, cells were resuspended in 300 µl of DPBS and aliquoted into two individual wells of a 96-well microplate with or without supplementing dopamine or GABA. Fluorescence excitation and emission spectra were next determined on a BioTek Synergy Mx plate reader.

Kinetic responses of the selected biosensors. Fluorescence intensities of purified SoNar, aY-SoNar, iNap1, aY-iNap1, iATPSnFR1.1 and aY-iATPSnFR1.1 proteins were measured by using a CLARIOstar Plus microplate reader (BMG Labtech) equipped with reagent dispensers. The excitation wavelength was set at 480 or 540 nm and the emission wavelength was set at 515 or 605 nm. Each kinetic measurement lasted 300 s and the interval between each reading was 1 s. To SoNar and aY-SoNar, NADH (at a final concentration of 10 µM) was injected at 60 s, and KP372–1 (at a final concentration of 1.5 µM; Echelon Biosciences Research Labs) and NAD(P)H:quinone oxidoreductase 1 (NQO1, at a final concentration of 3 μM; R&D Systems) were injected at 180 s. Similarly, to iNap1 and aY-iNap1, NADPH (at a final concentration of 10 μM) was injected at 60 s, and KP372−1 (at a final concentration of 1.5 μM) and NQO1 (at a final concentration of 3 μM) were injected at 180 s. Before measurement, iATPSnFR1.1 and aY-iATPSnFR1.1 were preincubated with 1x FastAP Reaction Buffer (Thermo Scientific). ATP (at a final concentration of 500 μM) was injected at 60 s, and 40 units of FastAP Alkaline Phosphatase (Thermo Scientific) was injected at 180 s. Recorded intensity values were corrected for volume changes and related instrument responses by using the sfGFP protein that is expected to be unresponsive to all of these chemical and enzymatic treatments.

Culture and transfection of mammalian cell lines. HEK 293T cells and HeLa cells (purchased from ATCC and tested for mycoplasma by PCR) were cultured in DMEM containing 1 g l^{-1} glucose and 10% fetal bovine serum (FBS) in a humidified 37 °C incubator with 5% CO_2. The day before transfection, 2.5×10^5 cells were used to seed each 35-mm cell culture dish. At the time of transfection, 10 μg of PEI (linear polyethylenimine, 25 kDa, from Polysciences) and a total of 4 μg of corresponding plasmid DNA (pcDNA3 biosensor plasmid/pMAH-aYRS, 1:1, w/w) were mixed in 250 μl of Opti-MEM I Reduced Serum Medium. Complexation lasted for 15 min at room temperature before addition of the mixture to cells with FBS-containing DMEM preremoved. After an additional 3 h of cell incubation at 37 °C, the Opti-MEM mixture was replaced with DMEM supplemented with 10% FBS and 2 mM aY. Cell culture media were replaced every 36 h. Fluorescence imaging was typically performed between 48 and 72 h post transfection. Mouse insulinoma MIN6 cells (a gift from S. Chen at Weill Cornell Medical College; tested for mycoplasma by PCR) were maintained in GlutaMAX-supplemented DMEM containing 4.5 g l^{-1} glucose, 10 mM HEPES (pH 7.4), 50 μM 2-mercaptoethanol and 10% FBS at 37 °C. The transfection procedure was similar to that of HEK 293T and HeLa, except for that 6×10^5 cells were used to seed each 35-mm cell culture dish, and that commercial Lipofectamine 2000 (Thermo Fisher) was used to replace PEI.

Culture and transfection of primary mouse hippocampal neurons. E18 mouse hippocampus was purchased from BrainBits. Dissociated neurons were cultured with 2 ml of NbActiv4 medium (BrainBits) in 35-mm glass-bottom dishes precoated with collagen I (catalog no. A1048301, Thermo Fisher). Every 2 d, half of the cell culture medium was replaced with fresh NbActiv4. Neurons were transfected on day 7 by following BrainBits's protocol. Briefly, 1 ml of culture medium was taken from each 35-mm dish and combined with another 1 ml of fresh NbActiv4. The conditioned medium was incubated at 37 °C and 5% CO_2. A total of 4 μg of plasmid DNA (G-GECO1/aY-iGluSnFR/pMAH-aYRS, 1:2:2, w/w/w) and 8 μl of Lipofectamine 2000 (Thermo Fisher) were mixed in 100 μl of BrainBits Transfection Medium and the resultant mixture was incubated at room temperature for 15 min. Next, 1 ml of warm, conditioned NbActiv4 medium was used to replace the medium in each 35-mm dish and the transfection mixture was then added. After 3 h of incubation at 37 °C in a 5% CO_2 incubator, the medium was exchanged again to the conditioned medium without transfection mixture but supplemented with 2 mM aY. Half of the aY-containing medium was exchanged every 2 d. Fluorescence imaging was performed between 48 and 72 h post transfection.

Time-lapse imaging of aY-GECO1, aY-PercevalHR, aY-iATPSnFR and aY-SoNar in HeLa. For aY-GECO1, HeLa cells in DPBS (Ca^{2+}- and Mg^{2+}-free) were imaged every 1 s for a duration of 13 min. Stimuli, such as 5 μM histamine, 1 mM $CaCl_2$ with 10 μM ionomycin, and 2 mM EGTA with 5 μM ionomycin, were added sequentially. For aY-PercevalHR or aY-iATPSnFR, HeLa cells in Ca^{2+}- and Mg^{2+}-containing Hank's balanced salt solution (HBSS) were imaged every 30 s and 10 mM 2-DG was added to induce cellular ATP concentration changes. For aY-SoNar, HeLa cells in Ca^{2+}- and Mg^{2+}-containing DPBS were imaged every 20 s and 1 mM sodium pyruvate was added as the stimulus.

Time-lapse imaging of aY-ZnGreen1 and aY-iNap1 in HEK 293T. For aY-GECO1, HEK 293T cells in modified Krebs-HEPES-bicarbonate buffer (KHB) containing 140 mM NaCl, 3.6 mM KCl, 0.5 mM NaH_2PO_4, 0.5 mM $MgSO_4$, 1.5 mM $CaCl_2$, 10 mM HEPES, 2 mM $NaHCO_3$ and 3 mM glucose were imaged every 4 s. $ZnCl_2$ stock was prepared in slightly acidic pure water. TPEN and pyrithione stock solutions were prepared in DMSO. KHB was then used to dilute Zn^{2+}, pyrithione and TPEN to desired concentrations right before each use. For aY-iNap1, HEK 293T cells in DPBS were imaged every minute. Diamide (1 mM) was used to stimulate NADPH changes.

Imaging of metabolic dynamics of MIN6 cells. Cells were transiently transfected as described in the "Culture and transfection of mammalian cell lines" section with desired combinations of plasmids and imaged between 48 and 72 h post transfection. Before imaging, cells were washed thoroughly and left in HBSS (1 g l^{-1} glucose) for 1-h starvation. Images were acquired every minute. D-glucose (20 mM) was added to stimulate MIN6 cells.

Data and statistical analysis. Fiji was used to analyze microscopic images. Microsoft Excel, OriginPro, GraphPad Prism and Affinity Designer were used to analyze data and prepare figures for publication. The Wilcoxon matched-pairs signed rank test was used to determine the *P* value. No sample was excluded from data analysis, and no blinding was employed. Unless otherwise indicated, data are shown as mean and standard deviation, and error bars in figures represent standard deviation.

Reporting Summary. Further information on research design is available in the Nature Research Reporting Summary linked to this article.

Data availability

The gene sequences for *Mj*aYRS and *Ec*aYRS have been deposited to GenBank under the accession numbers MT002434 and MT002433, respectively. The plasmids for pEvol-*Mj*aYRS (Plasmid no. 153557) and pMAH-*Ec*aYRS (Plasmid no. 153558) have been deposited to Addgene. Materials, associated protocols and other supporting data are available from the corresponding author upon request. Source data are provided with this paper.

References

51. Trott, O. & Olson, A. J. AutoDock Vina: improving the speed and accuracy of docking with a new scoring function, efficient optimization, and multithreading. *J. Comput. Chem.* **31**, 455–461 (2010).
52. Young, T. S., Ahmad, I., Yin, J. A. & Schultz, P. G. An enhanced system for unnatural amino acid mutagenesis in *E. coli*. *J. Mol. Biol.* **395**, 361–374 (2010).
53. Zhang, Z. & Marshall, A. G. A universal algorithm for fast and automated charge state deconvolution of electrospray mass-to-charge ratio spectra. *J. Am. Soc. Mass Spectrom.* **9**, 225–233 (1998).
54. Kobayashi, T. et al. Structural basis of nonnatural amino acid recognition by an engineered aminoacyl-tRNA synthetase for genetic code expansion. *Proc. Natl Acad. Sci. USA* **102**, 1366–1371 (2005).
55. Chatterjee, A., Xiao, H., Bollong, M., Ai, H. W. & Schultz, P. G. Efficient viral delivery system for unnatural amino acid mutagenesis in mammalian cells. *Proc. Natl Acad. Sci. USA* **110**, 11803–11808 (2013).
56. Kellogg, R. E. & Bennett, R. G. Radiationless intermolecular energy transfer. III. Determination of phosphorescence efficiencies. *J. Chem. Phys.* **41**, 3042–3045 (1964).
57. Bindels, D. S. et al. mScarlet: a bright monomeric red fluorescent protein for cellular imaging. *Nat. Methods* **14**, 53–56 (2017).

Acknowledgements

We thank R. Campbell, L. Looger, B. Khakh, G. Yellen and P. Schultz for plasmids; S. Chen for MIN6 cells; and other members of the Ai laboratory for discussion and assistance with experiments. We thank W. Ren and A. Ji for early exploration of this project. Research reported in this publication was supported in part by the University of Virginia and the National Institutes of Health under awards nos. R01GM118675, R01GM129291, U01CA230817 and R01DK122253.

Author contributions

H.-w.A. conceived and supervised the project. S.Z. performed all experiments. H.-w.A. and S.Z. analyzed the data and prepared the manuscript.

Competing interests

The authors declare no competing interests.

Additional information

Extended data is available for this paper at https://doi.org/10.1038/s41589-020-0641-7.

Supplementary information is available for this paper at https://doi.org/10.1038/s41589-020-0641-7.

Correspondence and requests for materials should be addressed to H.-w.A.

Reprints and permissions information is available at www.nature.com/reprints.

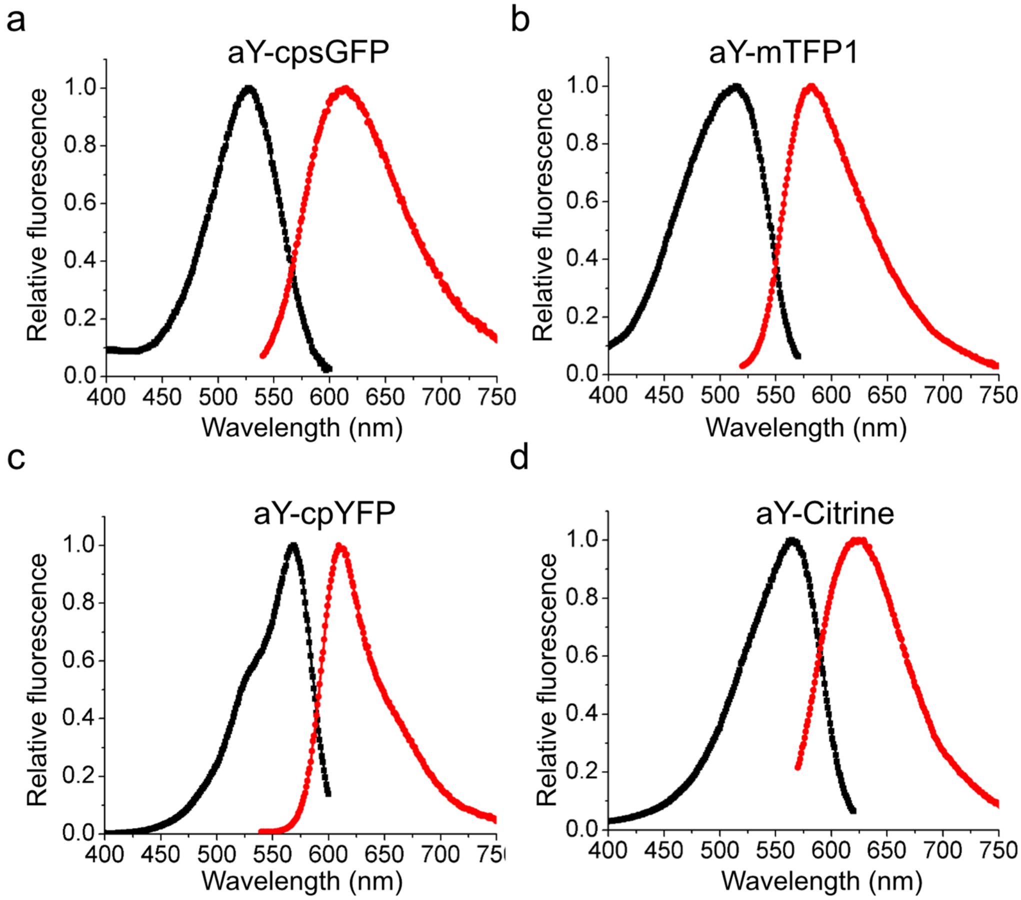

Extended Data Fig. 1 | Fluorescence excitation and emission of aY-modified fluorescence proteins. Fluorescence excitation (black) and emission (red) profiles of aY-modified cpsGFP **a**, mTFP1 **b**, cpYFP **c**, and Citrine **d**.

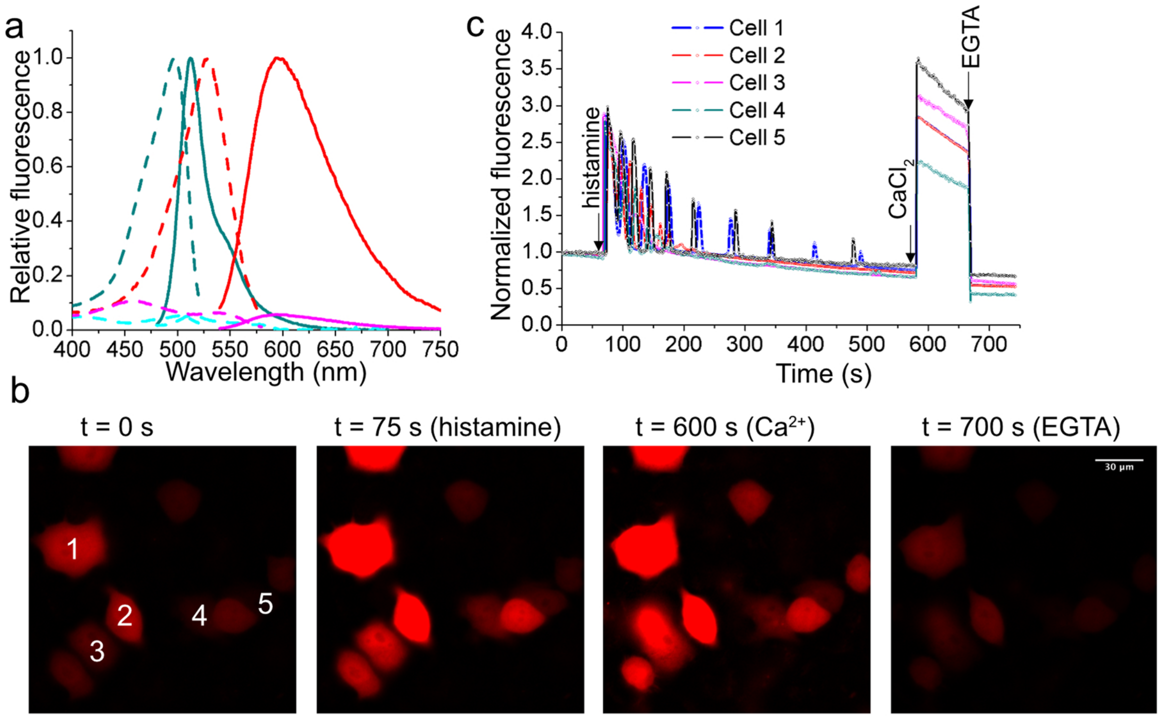

Extended Data Fig. 2 | Characterization of aY-modified G-GECO1 (Ca^{2+} sensor). a, Fluorescence excitation (dash line) and emission (solid line) profiles for G-GECO1 after addition of 1 mM EGTA (cyan) or 100 μM Ca^{2+} (dark cyan), and aY-G-GECO1 after addition of 1 mM EGTA (magenta) or 100 μM Ca^{2+} (red). **b**, Representative images of HeLa cells expressing aY-G-GECO1 in response to sequential addition of 5 μM histamine, 1 mM $CaCl_2$ with 10 μM ionomycin, and 2 mM EGTA with 5 μM ionomycin. Scale bar: 30 μm. **c**, Quantitative traces for randomly selected five cells in panel **b**. Intensities are normalized to the values at $t = 0$ s. The time points for addition of chemicals are shown as arrows. Ca^{2+} oscillations in response to histamine were observed as expected. These experiments were repeated three times with similar results using independent biological samples.

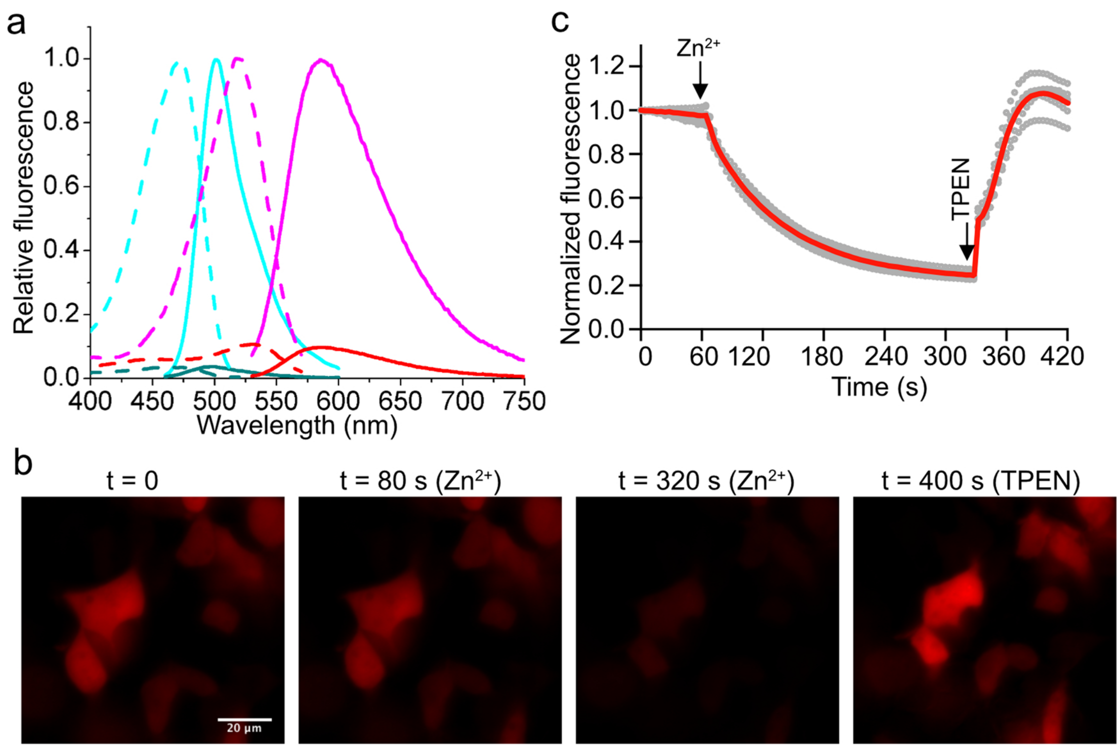

Extended Data Fig. 3 | Characterization of aY-modified ZnGreen1 (Zn^{2+} sensor). a, Fluorescence excitation (dash line) and emission (solid line) profiles for ZnGreen1 after addition of 1 mM EDTA (cyan) or 100 μM Zn^{2+} (dark cyan), and aY- ZnGreen1 after addition of 1 mM EDTA (magenta) or 100 μM Zn^{2+} (red). **b**, Representative images of HEK 293 T cells expressing aY-ZnGreen1 in response to sequential addition of 50 μM $ZnCl_2$ with 5 μM pyrithione, and 200 μM TPEN. Scale bar: 20 μm. **c**, Quantitative traces for randomly selected six single cells (gray dots) and their average (red line). Intensities are normalized to the values at $t = 0$ s. The time points for addition of chemicals are shown as arrows. These experiments were repeated three times with similar results using independent biological samples.

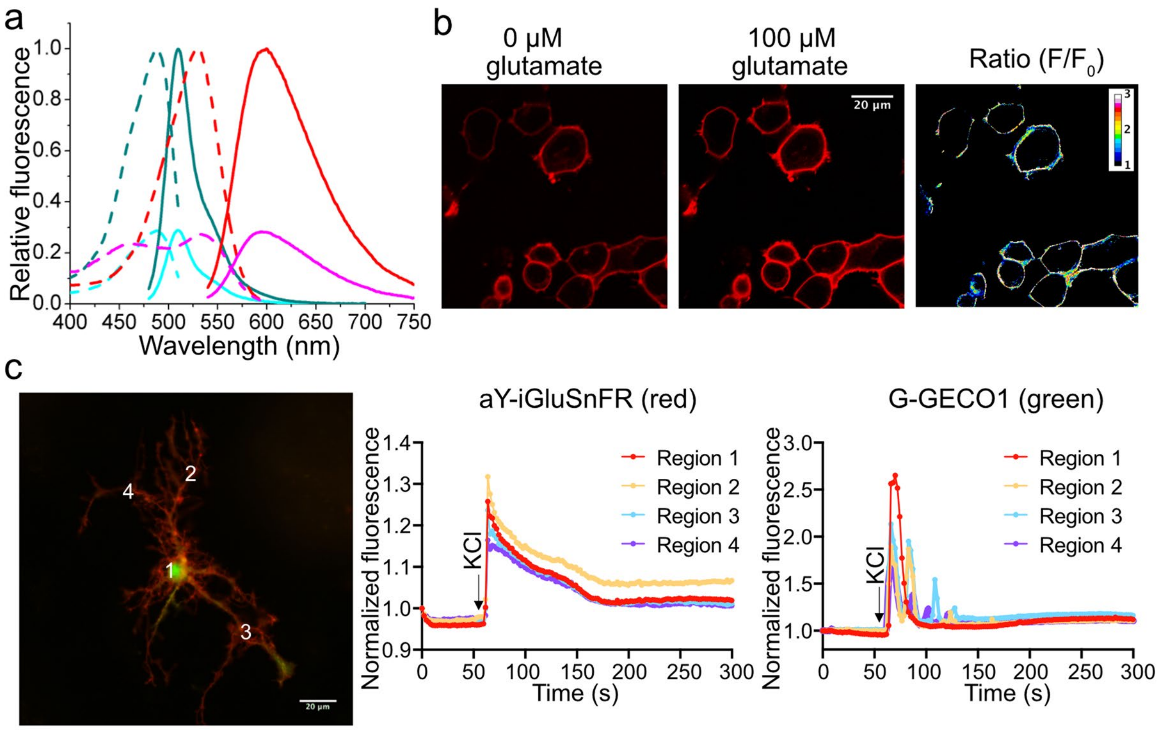

Extended Data Fig. 4 | Characterization of aY-modified iGluSnFR (glutamate sensor). a, Fluorescence excitation (dash line) and emission (solid line) profiles for iGluSnFR before (cyan) and after (dark cyan) addition of 100 μM L-glutamate, and aY-iGluSnFR before (magenta) and after (red) addition of 100 μM L-glutamate. **b**, Representative images of HEK 293 T cells expressing cell-surface-localized aY-iGluSnFR in response to addition of 100 μM L-glutamate. **c**, Cultured mouse hippocampal neurons in response to 90 mM KCl (excitatory Tyrode's saline buffer). Neurons were co-transfected to express cell-surface-localized aY-iGluSnFR (red fluorescence) and a Ca^{2+} indicator, G-GECO1 (green fluorescence). Quantitative traces for four different regions are presented. Intensities are normalized to the values at $t = 0$ s. These experiments were repeated three times with similar results using independent biological samples. Scale bar: 20 μm.

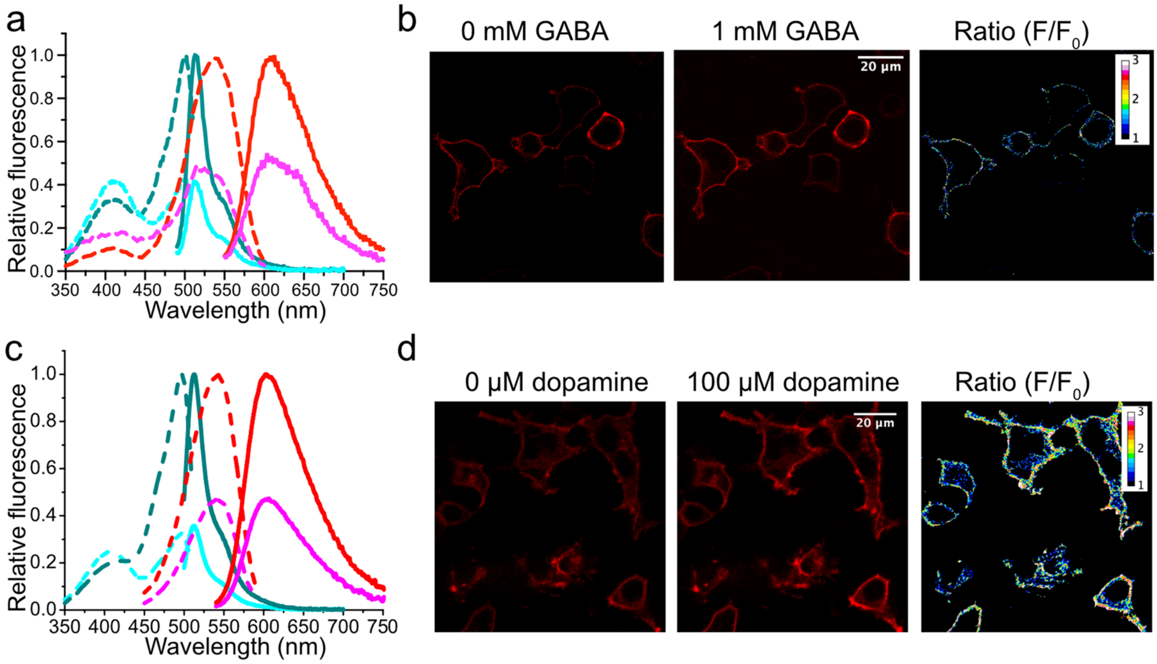

Extended Data Fig. 5 | Characterization of aY-modified iGABASnFR (a,b) and dLight1.2 (c,d) as biosensors for GABA and dopamine, respectively. **a**, **c**, Fluorescence excitation (dash line) and emission (solid line) profiles for iGABASnFR or dLight1.2 before (cyan) and after (dark cyan) addition of 1 mM GABA or 100 μM dopamine, and aY-iGABASnFR or aY-dLight1.2 before (magenta) and after (red) addition of 1 mM GABA or 100 μM dopamine. **b**, **d**, Representative images of HEK 293 T cells expressing surface-localized aY-iGABASnFR (**b**) or aY-dLight1.2 (**d**) in response to GABA or dopamine. These experiments were repeated three times with similar results using independent biological samples. Scale bar: 20 μm.

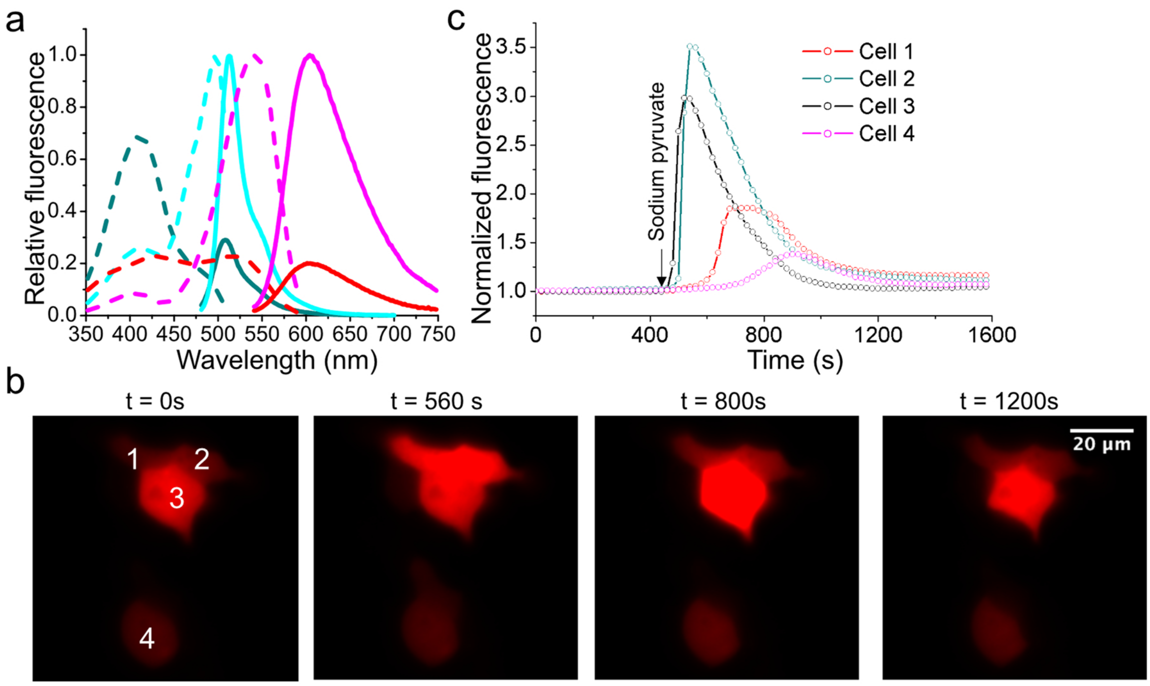

Extended Data Fig. 6 | Characterization of aY-modified SoNar (NAD⁺/NADH sensor). a, Fluorescence excitation (dash line) and emission (solid line) profiles for SoNar after addition of 20 µM NAD^+ (cyan) or NADH (dark cyan), and aY-SoNar after addition of 20 µM NAD^+ (magenta) or NADH (red). **b**, Representative images of HEK 293 T cells expressing aY-SoNar in response to addition of 1 mM pyruvate. Scale bar: 20 µm. **c**, Quantitative traces for randomly selected four single cells in panel b. Intensities are normalized to the values at $t = 0$ s. The time points for addition of chemicals are shown as arrows. These experiments were repeated three times with similar results using independent biological samples.

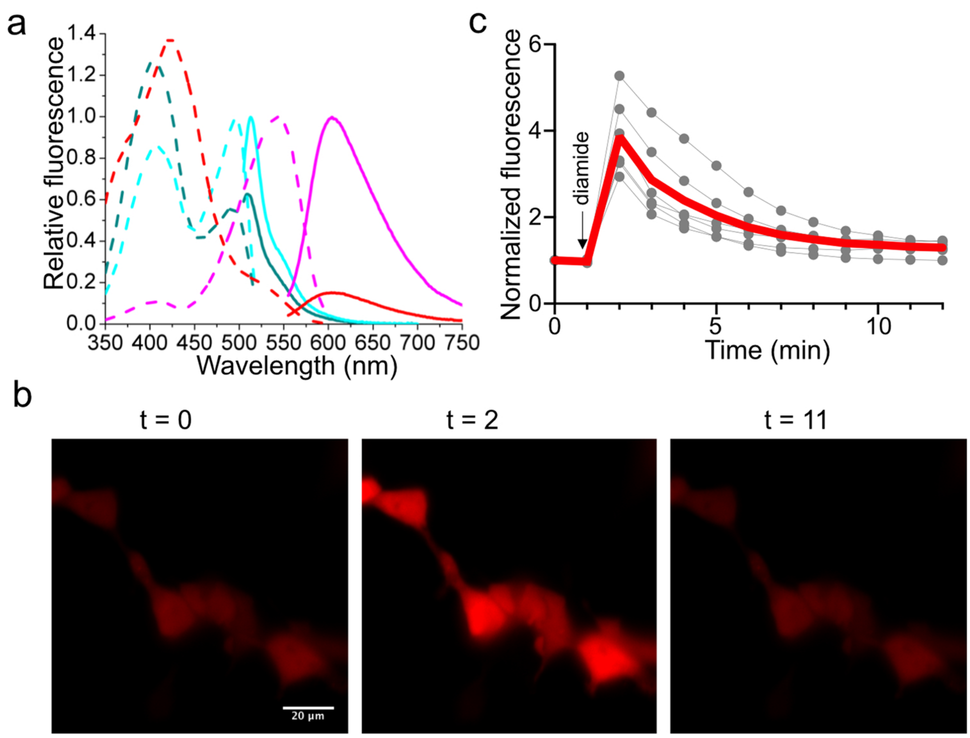

Extended Data Fig. 7 | Characterization of aY-modified iNap1 (NADPH sensor). **a**, Fluorescence excitation (dash line) and emission (solid line) profiles for iNap1 before (cyan) and after (dark cyan) addition of 100 µM NADPH, and aY-iNap1 before (magenta) and after (red) addition of 100 µM NADPH. **b**, Representative images of HEK 293 T cells expressing aY- iNap1 in response to addition of 1 mM diamide. Scale bar: 20 µm. **c**, Quantitative traces for randomly selected five single cells (gray dots) and their average (red line). Intensities are normalized to the values at $t=0$ s. The time points for addition of chemicals are shown as arrows. These experiments were repeated three times with similar results using independent biological samples.

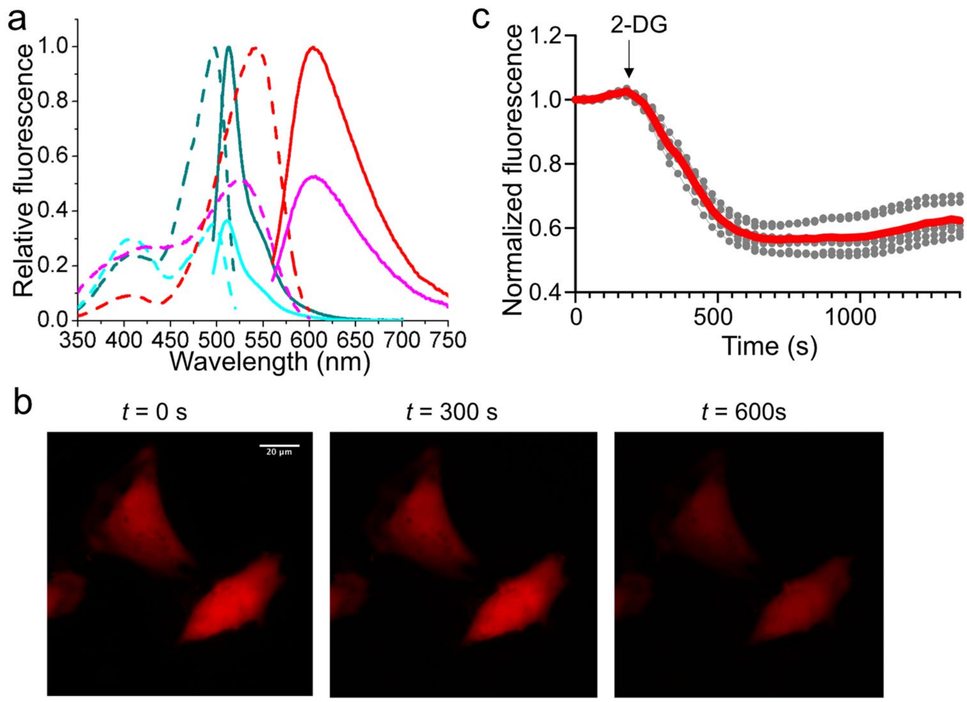

Extended Data Fig. 8 | Characterization of aY-modified PercevalHR (ATP sensor). a, Fluorescence excitation (dash line) and emission (solid line) profiles for PercevalHR before (cyan) and after (dark cyan) addition of 1 mM ATP, and aY-PercevalHR before (magenta) and after (red) addition of 1 mM ATP. **b**, Representative images of HeLa cells expressing aY- PercevalHR in response to 10 mM 2-deoxy-D-glucose (2-DG). Scale bar: 20 μm. **c**, Quantitative traces for randomly selected five single cells (gray dots) and their average (red line). Intensities are normalized to the values at $t = 0$ s. The time points for addition of chemicals are shown as arrows. These experiments were repeated three times with similar results using independent biological samples.

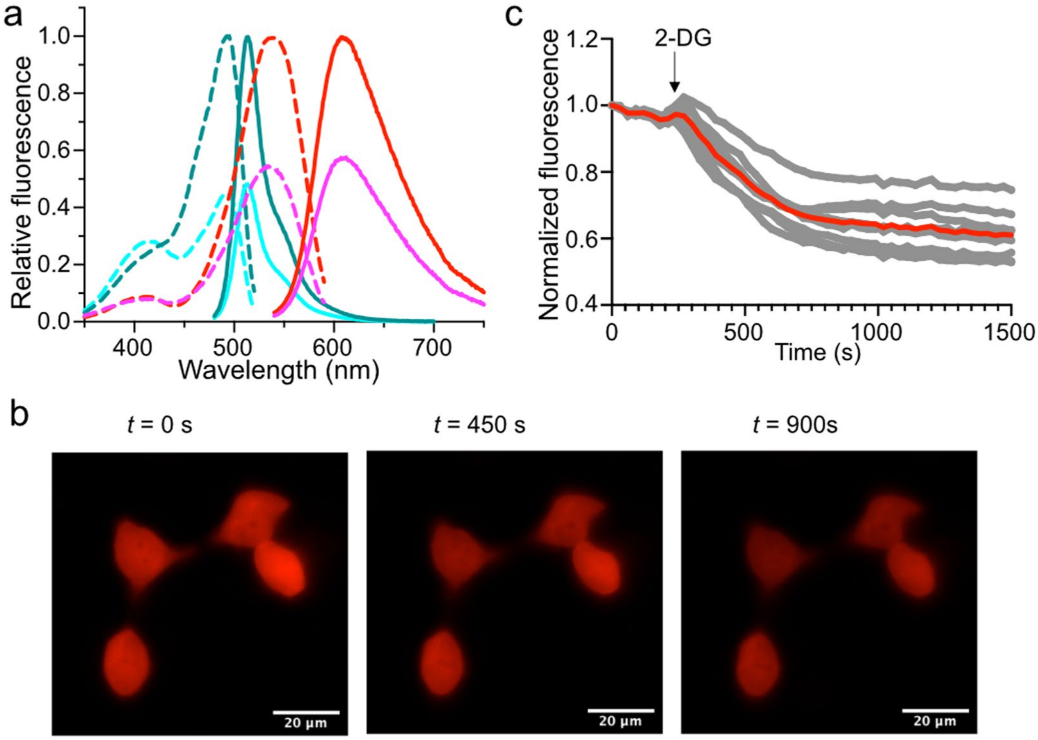

Extended Data Fig. 9 | Characterization of aY-modified iATPSnFR1.1 (ATP sensor). a, Fluorescence excitation (dash line) and emission (solid line) profiles for iATPSnFR1.1 before (cyan) and after (dark cyan) addition of 1 mM ATP, and aY-iATPSnFR1.1 before (magenta) and after (red) addition of 1 mM ATP. **b**, Representative images of HeLa cells intracellular expressing aY-iATPSnFR1.1 in response to 10 mM 2-deoxy-D-glucose (2-DG). Scale bar: 20 μm. **c**, Quantitative traces for randomly selected eight single cells (gray dots) and their average (red line). Intensities are normalized to the values at $t = 0$ s. The time points for addition of chemicals are shown as arrows. These experiments were repeated three times with similar results using independent biological samples.

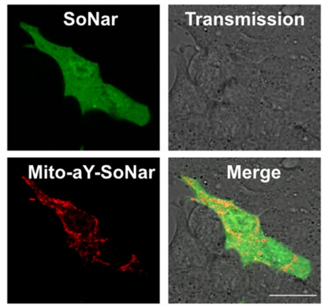

Extended Data Fig. 10 | Representative dual-color images of MIN6 cells co-expressing SoNar and mitochondrial aY-SoNar. MIN6 β-cells were sequentially imaged using GFP and RFP channels. Scale bar: 20 μm. This experiment was repeated three times independently with similar results.

nature research

Corresponding author(s): Hui-wang Ai

Last updated by author(s): Jul 20, 2020

Reporting Summary

Nature Research wishes to improve the reproducibility of the work that we publish. This form provides structure for consistency and transparency in reporting. For further information on Nature Research policies, see Authors & Referees and the Editorial Policy Checklist.

Statistics

For all statistical analyses, confirm that the following items are present in the figure legend, table legend, main text, or Methods section.

n/a	Confirmed	
☐	☒	The exact sample size (*n*) for each experimental group/condition, given as a discrete number and unit of measurement
☐	☒	A statement on whether measurements were taken from distinct samples or whether the same sample was measured repeatedly
☐	☒	The statistical test(s) used AND whether they are one- or two-sided *Only common tests should be described solely by name; describe more complex techniques in the Methods section.*
☒	☐	A description of all covariates tested
☒	☐	A description of any assumptions or corrections, such as tests of normality and adjustment for multiple comparisons
☐	☒	A full description of the statistical parameters including central tendency (e.g. means) or other basic estimates (e.g. regression coefficient) AND variation (e.g. standard deviation) or associated estimates of uncertainty (e.g. confidence intervals)
☐	☒	For null hypothesis testing, the test statistic (e.g. *F*, *t*, *r*) with confidence intervals, effect sizes, degrees of freedom and *P* value noted *Give P values as exact values whenever suitable.*
☒	☐	For Bayesian analysis, information on the choice of priors and Markov chain Monte Carlo settings
☒	☐	For hierarchical and complex designs, identification of the appropriate level for tests and full reporting of outcomes
☒	☐	Estimates of effect sizes (e.g. Cohen's *d*, Pearson's *r*), indicating how they were calculated

Our web collection on statistics for biologists contains articles on many of the points above.

Software and code

Policy information about availability of computer code

Data collection	Leica LAS X or Micro-Manager were used to collect microscopic images. BioTek Gen5 or BMG LABTECH CLARIOstar Plus Reader Control and MARS Data Analysis Software were used for fluorescence measurements. Waters MassLynx Mass Spectrometry Software was used for ESI-MS.
Data analysis	Fiji was used to analyze microscopic images. Microsoft Excel, OriginPro, GraphPad Prism, and Affinity Designer were used to analyze data and prepare figures for publication. PyMOL and AutoDock Vina were used for structural visualization and modeling. MagTran1.03 was used to deconvolve ESI-MS.

For manuscripts utilizing custom algorithms or software that are central to the research but not yet described in published literature, software must be made available to editors/reviewers. We strongly encourage code deposition in a community repository (e.g. GitHub). See the Nature Research guidelines for submitting code & software for further information.

Data

Policy information about availability of data

All manuscripts must include a data availability statement. This statement should provide the following information, where applicable:

- Accession codes, unique identifiers, or web links for publicly available datasets
- A list of figures that have associated raw data
- A description of any restrictions on data availability

The gene sequences for MjaYRS and EcaYRS have been deposited to GenBank under the accession numbers MT002434 and MT002433, respectively. The plasmids for pEvol-MjaYRS (Plasmid #153557) and pMAH-EcaYRS (Plasmid #153558) have been deposited to Addgene. The structures for the MjTyrRS mutant in complex with 3-iodotyrosine and the EcTyrRS mutant in complex with 3-iodotyrosine are available from the Protein Data Bank (PDB) under the accession numbers 2ZP1and 1WQ3, respectively. Materials, associated protocols, and other supporting data are available from the corresponding author upon request.

Field-specific reporting

Please select the one below that is the best fit for your research. If you are not sure, read the appropriate sections before making your selection.

☒ Life sciences ☐ Behavioural & social sciences ☐ Ecological, evolutionary & environmental sciences

For a reference copy of the document with all sections, see nature.com/documents/nr-reporting-summary-flat.pdf

Life sciences study design

All studies must disclose on these points even when the disclosure is negative.

Sample size	At least two or three independent experiments were conducted, analyzed, and summarized. Sample sizes were determined on the basis of previous experiments by considering biological/technical variability. No statistical methods were used to pre-determine the sample size.
Data exclusions	No data was excluded from data analysis.
Replication	All data reported in this study as biological replicates are stated in figure legends. All experiments were replicated at least two or three times. All repetitions were deemed successful.
Randomization	Cell cultures were randomly assigned to treatment groups.
Blinding	Blind was not relevant since no animal or human participants were used in this study.

Reporting for specific materials, systems and methods

We require information from authors about some types of materials, experimental systems and methods used in many studies. Here, indicate whether each material, system or method listed is relevant to your study. If you are not sure if a list item applies to your research, read the appropriate section before selecting a response.

Materials & experimental systems

n/a	Involved in the study	
☒	☐	Antibodies
☐	☒	Eukaryotic cell lines
☒	☐	Palaeontology
☒	☐	Animals and other organisms
☒	☐	Human research participants
☒	☐	Clinical data

Methods

n/a	Involved in the study	
☒	☐	ChIP-seq
☒	☐	Flow cytometry
☒	☐	MRI-based neuroimaging

Eukaryotic cell lines

Policy information about cell lines

Cell line source(s)	MIN6 cells was a gift from Dr. Shuibing Chen at Weill Cornell Medical College. HEK 293T cells and HeLa cells were purchased from ATCC.
Authentication	Not authenticated in our lab, but HEK and HeLa were directly purchased from ATCC.
Mycoplasma contamination	Cells were routinely tested for mycoplasma (every 2-3 months) and were always negative.
Commonly misidentified lines (See ICLAC register)	None of the cell lines used are listed in the current ICLAC database.